ChemPubSoc Europe
DOI: 10.1002/cssc.201500331
CHEMSUSCHEM
Full Papers

Acid-Functionalized Mesoporous Carbon: An Efficient Support for Ruthenium-Catalyzed γ-Valerolactone Production

Alberto Villa,[a] Marco Schiavoni,[a] Carine E. Chan-Thaw,[a] Pasquale F. Fulvio,[b, c] Richard T. Mayes,[c] Sheng Dai,[b, d] Karren L. More,[e] Gabriel M. Veith,[e] and Laura Prati*[a]

The hydrogenation of levulinic acid has been studied using Ru supported on ordered mesoporous carbons (OMCs) prepared by soft-templating. P- and S-containing acid groups were introduced by postsynthetic functionalization before the addition of 1% Ru by incipient wetness impregnation. These functionalities and the reaction conditions mediate the activity and selectivity of the levulinic acid hydrogenation. The presence of S-containing groups (Ru/OMC-S and Ru/OMC-P/S) deactivates the Ru catalysts strongly, whereas the presence of P-containing groups (Ru/OMC-P) enhances the activity compared to that of pristine Ru/OMC. Under mild conditions (70 °C and 7 bar H_2) the catalyst shows high selectivity to γ-valerolactone (GVL; $>95\%$) and high stability on recycling. However, under more severe conditions (200 °C and $p_{H_2}=40$ bar) Ru/OMC-P is particularly able to promote GVL ring-opening and the consecutive hydrogenation to pentanoic acid.

Introduction

γ-Valerolactone (GVL) has been identified as a potential sustainable platform molecule for the production of renewable fuels and fine chemicals.[1] Indeed, GVL can be used as a solvent,[1a] a part of a battery electrolyte,[2a] and to produce chemicals[1] and fuel additives in a similar capacity to ethanol.[1,2b–d] It can be converted to liquid fuels, namely, valeric biofuels and liquid alkanes[2] or to high-value chemical intermediates such as 1,4-pentanediol[3] or alkyl pentenoates, which are precursors to biopolymers.[4] Among the various products, pentanoic acid (PA) is a relevant intermediate for the formation of valeric biofuels that consist of pentanoic acid esters.[2]

The production of GVL is based mainly on the hydrogenation of levulinic acid (LA), which can be obtained directly from cellulosic materials by acidic hydrolysis.[1] A cascade reaction that involves hydrogenation and dehydration steps takes place under acidic conditions, and the order of these steps determines the overall reaction pathway (Scheme 1). For instance, LA can be reduced to 4-hydroxypentanoic acid (HPA) and then dehydrated to GVL (pathway a) or converted to angelica lactone (AL) by dehydration followed by reduction to GVL (pathway b).[5] These reactions take place in the presence of metallic catalysts, such as Ru[6] or Cu[7] supported on activated carbon (AC) or oxidic supports, in the presence of different solvents, such as water,[1,2] alcohols,[1,2] and dioxane.[8] It has been shown that by adding an acidic cocatalyst, such as niobium phosphate or oxide, to Ru/AC, it is possible to increase the reaction rate under mild conditions (70 °C, 3 bar of H_2) and maintain a selectivity $>98\%$ towards GVL.[9] This result has been attributed to the promotional effect of the acidic cocatalyst on the dehydration step (Scheme 1). Under more severe conditions (200 °C and 40 bar of H_2 pressure), it has been reported that Ru supported on acidic supports (H-beta or ZSM-5) promotes the ring-opening and hydrogenation of GVL to PA (Scheme 1).[6a] Similar results were reported by Dumesic et al. for Pd-supported Nb_2O_5 catalysts.[10]

This subsequent hydrogenation is of particular interest for the production of valeric biofuels from PA.[11] The major limitation of most of the heterogeneous catalysts applied in this reaction is their low stability. Herein we report Ru-supported on acid-functionalized ordered mesoporous carbon (OMC) as a catalyst that exhibits high activity, selectivity, and a long life-time for the hydrogenation of LA to GVL. Moreover, with the use of these catalysts, it is possible to tune the selectivity of the reaction by varying the reaction conditions. The activity and selectivity of the reaction to GVL or PA were correlated to the nature of the acidic groups.

---

[a] Dr. A. Villa, Dr. M. Schiavoni, Dr. C. E. Chan-Thaw, Prof. L. Prati
Dipartimento di Chimica
Università degli Studi di Milano
via Golgi 19, 20133 Milano (Italy)
E-mail: laura.prati@unimi.it

[b] Dr. P. F. Fulvio, Dr. S. Dai
Chemical Sciences Division
Oak Ridge National Laboratory
Oak Ridge, TN, 37831 (USA)

[c] Dr. P. F. Fulvio, Dr. R. T. Mayes
Department of Chemistry
University of Puerto Rico
Rio Piedras Campus, San Juan, PR 00931 (USA)

[d] Dr. S. Dai
Department of Chemistry
University of Tennessee
Knoxville, TN, 37996 (USA)

[e] Dr. K. L. More, Dr. G. M. Veith
Materials Science and Technology Division
Oak Ridge National Laboratory
Oak Ridge, TN 37831 (USA)

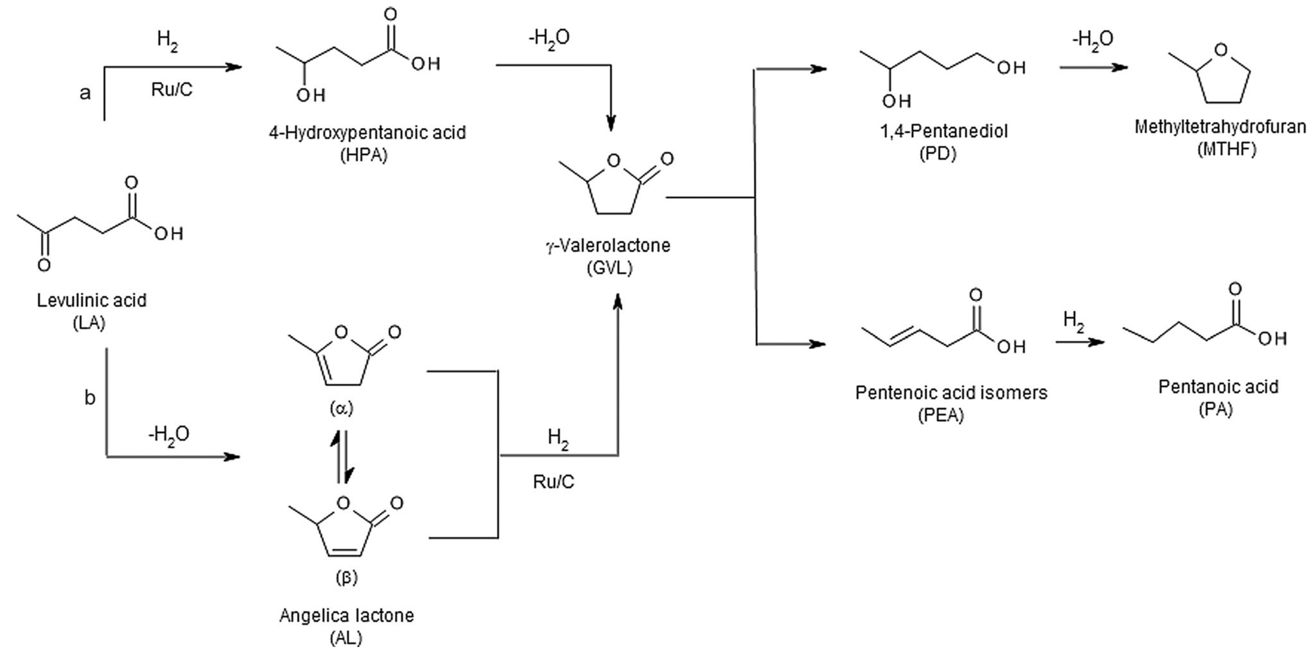

Scheme 1. Overall reaction pathway for the production of GVL.

Results and Discussion

OMCs synthesized using the soft-templating method under strongly acidic conditions exhibit large uniform mesopores and high specific surface areas.[12] OMCs are susceptible to surface modification with H_3PO_4 and H_2SO_4 with the retention of their porosities.[13] The OMC materials treated with H_3PO_4, H_2SO_4, and a mixture of H_3PO_4 and H_2SO_4 are labeled as OMC-P, OMC-S, and OMC-P/S, respectively.

As in previous reports, the OMC and functionalized OMCs exhibit type IV adsorption isotherms with steep capillary condensation steps and H_2 hysteresis loops characteristic of large cylindrical mesopores (Figure 1 a). The steepness of the capillary condensation steps indicates the uniformity of the mesopores in these materials. This was confirmed by the narrow pore size distributions calculated from the adsorption branch of these isotherms (Figure 1 b).[14]

The calculated adsorption and pore structures for all samples are summarized in Table 1. The specific surface area of the starting OMC was 589 $m^2 g^{-1}$ with a mean mesopore size of 8.7 nm. The introduction of acidic functional groups led to a decrease of the surface areas, and the lowest value was found for OMC-S/P (393 $m^2 g^{-1}$). The other two materials, OMC-P and OMC-S, had intermediate surface areas of 452 and 487 $m^2 g^{-1}$, respectively. The calculated mesopore widths of the modified carbons were similar to that of the starting OMC (8.2–8.4 nm). These findings are comparable to those for disordered mesoporous carbons modified with phosphoric acid, for which the adsorption properties were essentially retained after reaction with the mineral acid.[15]

Based on previous reports for the catalytic hydrogenation of GVL,[1,2,6a,9,17] the acidic properties play an important role to tune the activity (and selectivity) of the reaction. Therefore, the number of acidic sites on the catalyst surfaces was quantified

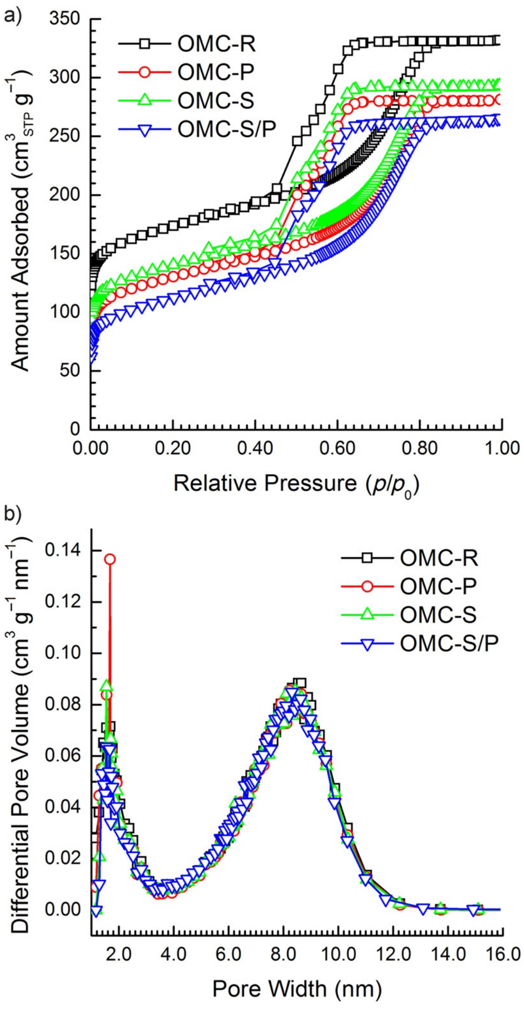

Figure 1. a) N_2 sorption isotherms and b) corresponding pore size distributions for the OMCs.

Table 1. Characteristics of the OMCs.

Sample	V_{SP}[a] [cm^3 g^{-1}]	V_{mi}–a_S plot[b] [cm^3 g^{-1}]	S_{mi}–a_S plot[c] [m^2 g^{-1}]	V_t–a_S plot[d] [cm^3 g^{-1}]	S_{ex}–a_S plot[e] [m^2 g^{-1}]	w_{KJS}[f] [nm]	S_{BET}[g] [m^2 g^{-1}]	Number of acid sites [mmol g^{-1}]
OMC	0.51	0.18	213	0.51	0.35	8.7	589	–
OMC-P	0.43	0.12	199	0.43	1.80	8.2	452	0.91
OMC-S	0.45	0.13	205	0.45	0.56	8.4	487	1.62
OMC-P/S	0.41	0.08	209	0.41	0.73	8.3	393	1.92

[a] Single-point pore volume from adsorption isotherms at p/p_0 ~0.98. [b] Micropore volume calculated in the standard relative adsorption (a_S) plot range of 0.75–1.00.[14] [c] Micropore surface area calculated in the a_S plot range of 0.75–1.00.[14] [d] Total pore volume calculated in the a_S plot range of 2.5–7.5.[14] [e] External surface area calculated in the a_S plot range of 2.5–7.5. [f] Pore width calculated according to the improved Kruk–Jaroniec–Sayari (KJS) method[15] using statistical film thickness for the nonporous carbon reference material.[16] [g] Specific surface area calculated using the Brunauer–Emmett–Teller equation in the relative pressure range of 0.05–0.20.

carefully by acid–base titration (Table 1). As expected, OMC-S/P has a higher number of surface acidic groups (1.98 mmol g^{-1}) than OMC-S (1.62 mmol g^{-1}) and OMC-P (0.91 mmol g^{-1}), whereas pristine OMC showed no acid character.

After Ru was deposited on the different supports by the incipient wetness impregnation technique, the morphology of the Ru nanoparticles was investigated by scanning transmission electron microscopy (STEM). Representative images of OMC and OMC/P are presented in Figure 2 a and b, respectively. The images showed that Ru is well dispersed on the supports and very small nanoparticles were obtained with a mean diameter of 1.3–1.8 nm (Table 2). This indicates that the different functional groups on the surface did not affect the Ru particle size significantly. Notably, the Ru particle size did not change after pretreatment at 150 °C before the reaction.

Table 2. Statistical median and standard deviation of particle size analysis for 1 % Ru catalysts obtained by STEM.

Samples	Statistical median [nm]	Standard deviation [σ]
Ru/OMC	1.3	0.5
Ru/OMC-P	1.6	0.6
Ru/OMC-P/S	1.5	0.6
Ru/OMC-S	1.8	0.7
Ru/OMC-P$_{\text{after reaction}}$	2.5	1.1

X-ray photoelectron spectroscopy (XPS) of the different supports and Ru-loaded catalysts (before activation) confirmed the successful functionalization of the OMC surfaces with P- and S-containing groups. The chemical species observed on the surface, their concentration, and the overall elemental composition are summarized in Table 3. The data show that the pristine OMC material has ≈8.3 at % oxygen on the surface of the

Table 3. XPS analysis.

Sample	Binding energy [eV] (peak area [%])											Elemental composition [at %] (C–O–P–S–Ru)
	C 1s					O 1s		P 1s	S 2p		Ru 3d$^{5/2}$	
	C–C, C–H	C–O, C–P,	C=O	O$^-$, C=O	C$^+$, C=C	C=O, P–O, P=O	C–O C–O–C P–O–C S–O	C–O–PO$_3$	–S	–SO$_4$		
OMC	284.8 (59.1)	286.5 (26.0)	288.5 (7.3)	290.4 (5.0)	292.1 (2.6)	532.3 (12)	533.7 (88)					91.7–8.3–0–0–0
OMC-P	284.8 (65.9)	286.4 (17.5)	288.4 (7.3)	290.3 (5.8)	292.2 (3.5)	531.2 (10.4)	532.9 (89.6)	134.2 (100)				91.2–8.4–0.4–0–0
OMC-S	284.8 (65.8)	286.4 (16.8)	288.4 (7.6)	290.2 (5.7)	292.1 (4.1)	532.2 (35.1)	533.3 (64.9)			169.1 (100)		89.8–9.8–0–0.4–0
OMC-S/P	284.8 (65.8)	286.4 (16.9)	288.4 (7.5)	290.3 (5.9)	292.1 (3.8)	531.9 (65.1)	533.4 (34.9)	134.4 (100)		169.0 (100)		89.1–10.2–0.3–0.4–0
Ru/OMC	284.8 (61.4)	286.3 (23.8)		289.1 (9.0)	291.5 (5.8)	532.1 (71.5)	533.8 (28.5)				281.4 (100)	91.6–6.3–0–0–1.9
Ru/OMC-P	284.8 (67.0)	286.3 (13.1)	288.0 (12.2)		290.6 (7.7)	531.5 (18.3)	533.1 (81.7)	134.9 (100)			281.4 (100)	88.2–10.6–0.7–0–0.4
Ru/OMC-S	284.8 (69.9)	286.4 (11.4)	288.0 (10.8)	290.2 (6.0)	291.9 (1.9)	531.3 (31.9)	533.1 (68.1)		163.7 (33.1)	168.9 (66.9)	281.4 (100)	87.8–11.3–0–0.4–0.5
Ru/OMC-P/S	284.8 (64.9)	286.3 (13.4)	288.1 (12.9)		290.7 (8.8)	531.7 (30.7)	533.3 (69.3)	134.8 (100)		169.2 (100)	281.5 (100)	88.1–10.7–0.5–0.1–0.6
Ru/OMC-P$_{\text{used (at 200 °C)}}$	284.8 (70.5)	286.9 (11.1)	288.8 (12.5)		291.3 (6.0)	532.4 (76.2)	533.7 (23.8)	134.2 (100)			280.4/ 283.4 (50/50)	89.9–8.6–0.2–0–1.2
Ru/OMC-S$_{\text{used (at 70 °C)}}$	284.9 (68.2)	286.3 (11.0)	287.7 (10.7)	289.3 (6.9)	291.4 (3.1)	531.8 (51.0)	533.5 (49.0)		163.7 (70.1)	168.5 (29.9)	281.4 (100)	88.0–11.0–0.1–1.4–0.6

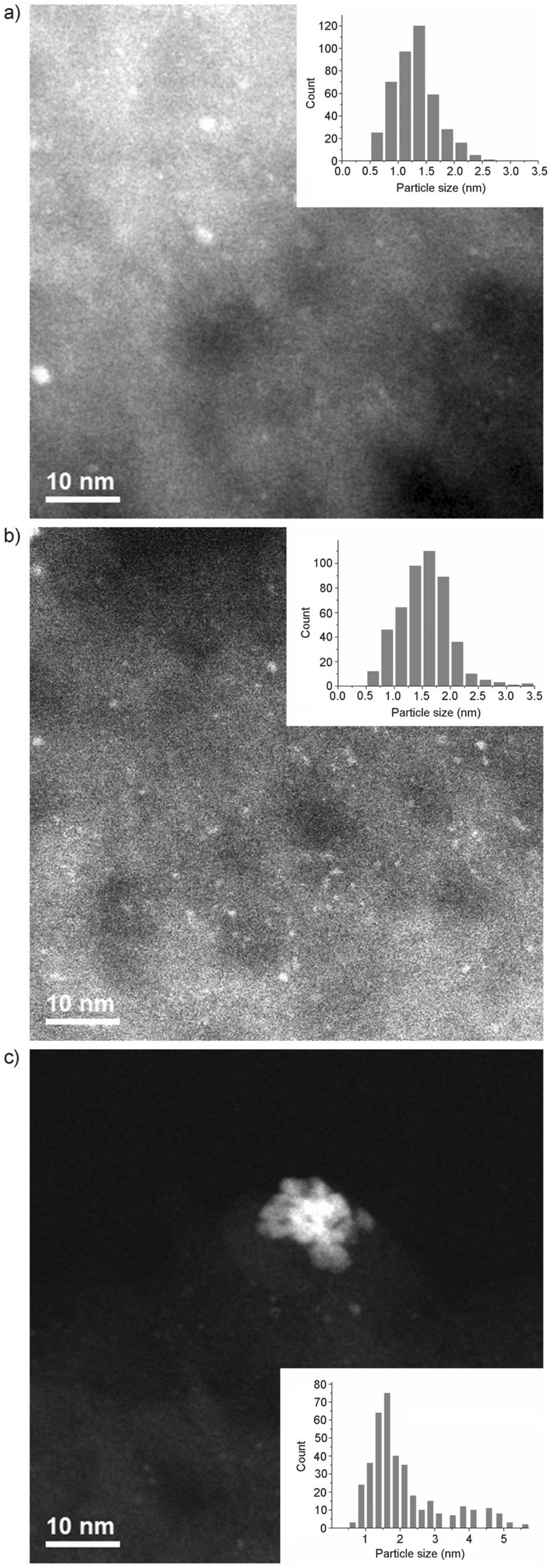

Figure 2. Representative STEM images of a) Ru on OMC, b) Ru on P-OMC, and c) Ru on P-OMC after reaction at 200 °C.

carbon. The oxygen chemistry is dominated by the presence of C–O groups as evidenced by the large signal at a binding energy (BE) of 286.5 eV (Figure 3, top) and the high BE observed for the O 1s species (533.7 eV). After the OMC was reacted with H_3PO_4 or H_2SO_4, $-OPO_3$ and $-OSO_3/-S$ species were identified on the carbon surfaces (BE = 134.2 and 169.0/163.7 eV, respectively) with a corresponding decrease in C–O concentration (BE ≈ 286.4 eV), which is evident if we compare the spectra of the pristine support materials with those of the materials that contain Ru (labeled as-prepared, 150 °C, or used, which depends on the state of the catalyst; Figure 3 top left and Table 3).

This decrease in the C–O signal compared to that of the original OMC material indicates a preferential reaction of the C–O species with the mineral acids. The concentration of P and S from the P–O and S–O groups are both around 0.4 at %, but there is a small increase in the total oxygen content because of the P–O and S–O species that replace the surface C–O.

After impregnation, the oxidation state of the Ru particles appears to be higher than +4. The exact oxidation state is difficult to determine because the overlap with the C 1s signal and the low Ru concentration on the catalysts with P- and S-containing groups. Indeed, a higher concentration of Ru was measured on the surface of the OMC material (1.9 at %) than on OMC-P and OMC-S (0.4 and 0.6 at %, respectively; Table 3). As the loading and the Ru particle sizes are similar in all the prepared catalysts, the lower Ru concentration on OMC-P, OMC-S, and OMC-P/S is probably because Ru is pulled into the pores. This could be caused by the preferential reaction of the apparent C–O nucleation sites by the acid groups or changes in hydrophobicity with acid treatment. Regardless, this effectively lowers the Ru content on the outer surface of the OMC support.

Before the materials were used as catalysts, they were reduced at 150 °C under $p_{H_2} = 3$ bar. To probe the resulting material, the same catalysts were reduced in 4 % H_2/Ar at 150 °C in a specially designed furnace contained within an Ar-filled glovebox. Although the reaction conditions are not identical, they are a good approximation for the expected reaction at high pressures given the reactivity of H_2. The reduced samples were stored in an Ar-filled glovebox and transferred to the XPS spectrometer in a vacuum-transfer case, designed to prevent any reoxidation process. Representative XPS data collected for the reduction of Ru/OMC, Ru/OMC-P, Ru/OMC-P-S, and Ru-OMC-S are shown in Figure 3. After the H_2 treatment, there is a clear shift in the Ru 3d$^{5/2}$ BE to lower energies (from 282.7 to 281.4 eV). This shift is caused by a reduction of the Ru, though this reduction does not seem to result in a total reduction to Ru^0. Instead, these BEs are consistent with the stabilization of oxidized Ru species with oxidation states around +4.[17,18] To characterize the Ru oxidation state further, we investigated the Ru 3p spectra for the OMC-supported material that had the highest surface content of Ru.

Fits of the Ru 3p XPS data show that the dominant species has a BE around 462 eV (Figure 4). This species is attributed to Ru^{4+}, most likely a result of RuO_2-type oxides, which are the

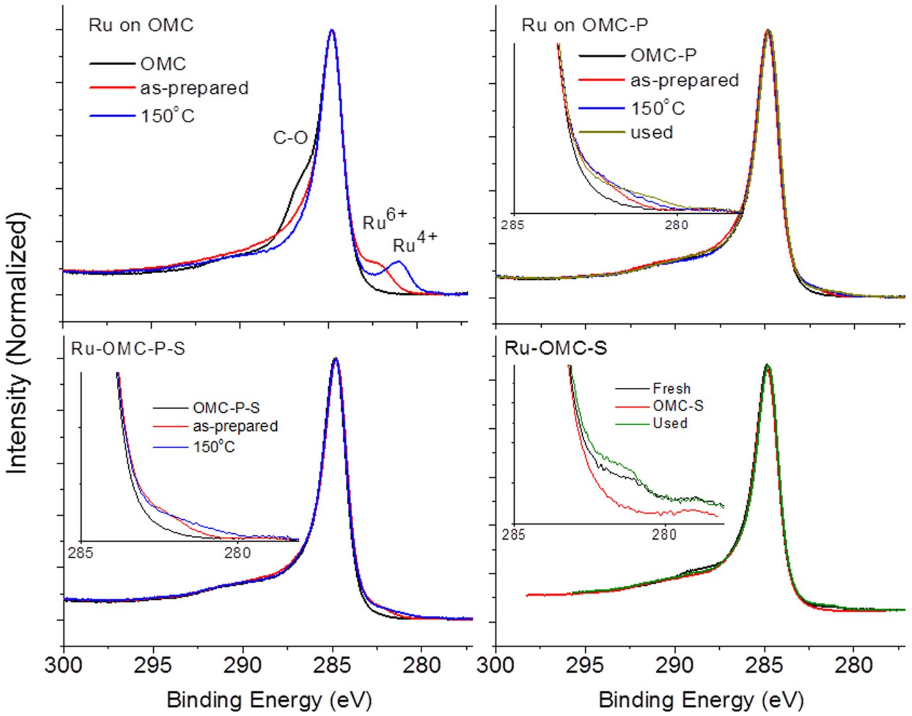

Figure 3. C1 s/Ru 3d XPS data collected for OMC (top left), OMC-P (top right), OMC-S (bottom right), and OMC-P-S (bottom left) catalyst supports (black), the as-prepared Ru catalysts (red), the Ru catalysts after reduction at 150 °C, and the Ru-OMC-P catalyst used at 150 °C (green).

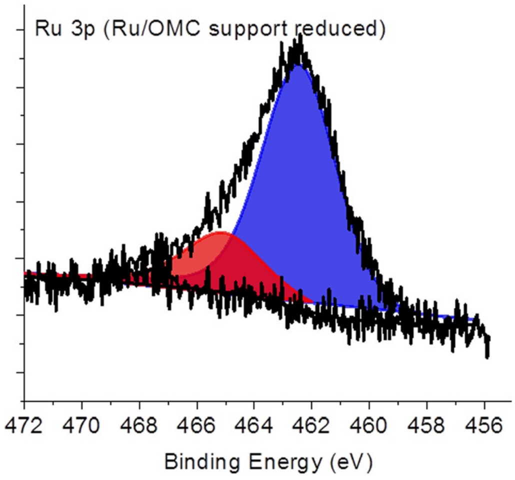

Figure 4. Ru 3p XPS data collected for the Ru/OMC catalyst after treatment at 150 °C and p_{H_2} 3 bar, consistent with Ru^{4+}.

Table 4. LA hydrogenation over 1% Ru-based catalysts at 70 °C and p_{H_2} = 7 bar.[a]

Catalysts	t [h]	Conversion [%]	Activity[b]	Selectivity [%] GVL	PEA	PA	PD	MTHF
Ru/OMC	3	32	1.05	98	0	0	0	0
	6	54	0.89	97	0	0	0	0
	9	65	0.72	98	0	0	0	0
Ru/ OMC-P	3	59	1.95	96	0	2	0	1
	6	98	1.61	94	1	3	0	1
	9	> 99	1.10	93	1	4	0	1
Ru/ OMC-S/P	3	15	0.49	98	0	0	0	1
	6	18	0.30	96	1	2	0	1
	9	20	0.22	95	1	2	0	1
Ru/ OMC-S	3	5	0.17	97	0	2	0	1
	6	8	0.13	95	0	3	0	0
	9	9	0.10	96	0	3	0	0

[a] Reaction: [LA] = 0.43 mol L^{-1}; Ru/LA = 1:1000 mol/mol. [b] Converted mol$_{GVL}$ g$_{Ru}$$^{-1}$ h^{-1}.

most stable oxides, and confirms the assignment from the Ru 3d data.[17,18] The second highest energy species, located at BE = 465 eV, is likely caused by water bound to the surface or a second, higher oxidation state Ru species, which was observed on the as-prepared catalysts. The reduction treatment had no clear influence on the –P–O chemistry but it changed the S functionality dramatically. Postsynthesis, there was a clear partial reduction of the –SO$_4$ group (BE = 169.1 eV) to result in the formation of a surface sulfide (BE = 163.7 eV).

The influence of the functionalization of the support on the catalytic performance was first investigated at 70 °C and 7 bar H_2 using water as the solvent ([LA] = 0.43 mol L^{-1}; Ru/LA molar ratio 1:1000 mol/mol; Table 4). The catalysts were pretreated under 3 bar H_2 at 150 °C.

The catalytic results are summarized in Table 4. After 9 h of reaction, only Ru/OMC-P reached full conversion, whereas conversions of 65, 20, and 9% were achieved with Ru/OMC, Ru/OMC-S/P, and Ru/OMC-S, respectively. The superior activity of Ru/OMC-P is in agreement with the positive effect on the catalytic performance ascribed to the presence of acidic groups and/or an acid cocatalyst. Indeed, the mixing of Ru/AC with an Amberlyst acidic resin[9] or an acidic oxide as the cocatalyst[19] enhanced the catalyst activity in LA hydrogenation by a factor of two.

A similar effect was reported for Ru supported directly on acidic resins.[20] A possible explanation could be the reaction pathway. Under mild reaction conditions, LA hydrogenation proceeds with the formation of 4-hydroxypentanoic acid followed by the intramolecular esterification to GVL (Pathway a, Scheme 1).[5,9] The presence of acidic groups increases the reaction rate to favor the acid-catalyzed esterification reaction of the intermediate γ-hydroxyvaleric acid to GVL.[9]

The promotional effect of phosphonic acid groups was not observed for S-containing catalysts. Indeed, a strong deactivation was observed with a virtually unchanged conversion at 3, 6, and 9 h of reaction. These results differ from those reported for Ru deposited on a sulfonic resin.[20] A possible explanation for such differences is in the various types of S-containing groups on the carbon surfaces and on their distinct stabilities compared to the most stable sulfonic groups found in resins (–Ph–SO_3H). In the case of the Ru OMC-S catalysts, XPS analysis after catalytic reduction showed a clear increase in the concentration of reduced sulfide species (BE = 163.7 eV; Figure 5). This indicates that some of the $-SO_4$ reacts under hydrogenation conditions. These reduced S-containing groups likely redeposited on Ru nanoparticles during the reaction, which thus blocks the metal active sites. Indeed, the strong binding properties of S-containing groups on the active site of the metal have been reported widely, in particular, for gas-phase reactions.[21]

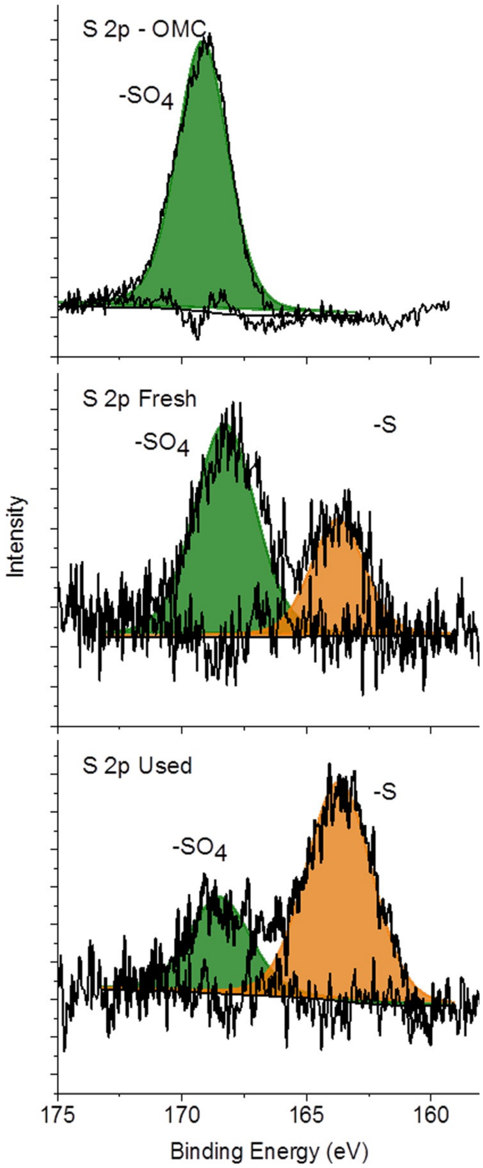

Figure 5. S 2p XPS data collected for OMC-S and 1 % Ru/OMC-S fresh and after reaction.

Despite their effect on catalytic activity, the presence of P- or S-containing groups did not significantly affect the selectivity under the reaction conditions (70 °C, 7 bar H_2). For all the catalysts, a selectivity higher than 94 % was achieved, and only traces of products derived from the consecutive GVL transformation [pentenoic acid (PEA), pentanoic acid (PA), 1,4-pentanediol (PD), methyltetrahydrofuran (MTHF)] were detected (Table 4).

A comparison of Ru/OMC and Ru/OMC-P at iso-conversion (54 and 59 %; Table 4), showed a comparable selectivity to GVL (97 and 96 %; Table 4).

Finally, recycling tests were performed to investigate the durability of the catalyst. These tests consisted of the filtration and reuse of the catalyst for the next run without any further purification. The catalyst showed a good stability with maintained activity and selectivity to GVL during the tests (Figure 6). Inductively coupled plasma (ICP) analysis of the collected solution after five runs did not show any significant Ru leaching (< 1 %). Moreover, STEM and BET analysis did not reveal any evident modification of the catalyst morphology.

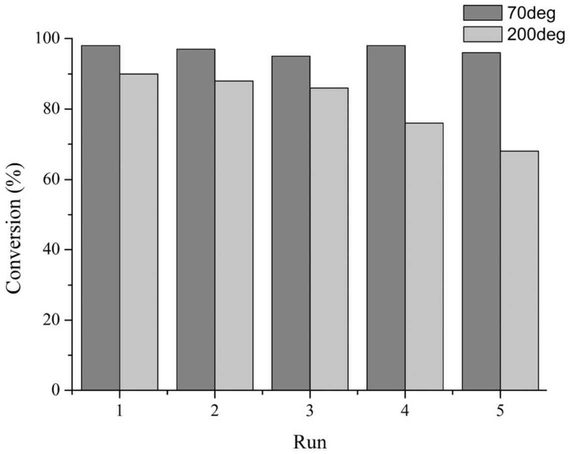

Figure 6. Stability test using 1 % Ru/OMC-P at 70 °C and 7 bar (6 h of reaction each cycle; dark gray) and at 200 °C and 40 bar (2 h of reaction each cycle; light gray).

More severe reaction conditions (200 °C, 40 bar H_2) improved the activity of both Ru/OMC and Ru/OMC-P. For instance, Ru/OMC reached full conversion after 6 h, whereas Ru/OMC-P showed a conversion of 90 % after only 2 h of reaction (Table 5). Moreover, Ru/OMC maintained a high selectivity (95 %) to GVL at full conversion even under more extreme reaction conditions, and acidic Ru/OMC-P converted GVL partially to pentanoic acid (10 % selectivity at 90 % conversion). The conversion of GVL to PA was further increased by simply prolonging the reaction time, and the selectivity to PA increased to 35 % after 10 h. Under similar reaction conditions, with the use of 2-ethylhexanoic acid instead of water as the solvent, Luo et al. compared different Ru supported on acid oxide catalysts, and the highest selectivity to PA was 15 % after 10 h of reaction over Ru/H-ZSM5.[6a] Therefore, Ru/OMC-P seems to be a promising catalyst to convert LA to PA just by tuning the re-

Table 5. LA hydrogenation over 1% Ru-based catalysts at 200 °C and p_{H_2} 40 bar.[a]

Catalyst	t [h]	Conversion [%]	Activity[b]	Selectivity [%] GVL	PEA	PA	PD	MTHF
Ru/OMC	2	79	3.91	96	0	0	0	1
	4	>99	2.48	95	1	0	0	2
Ru/OMC-P	2	90	4.46	85	4	10	0	2
	3	>99	3.30	75	1	22	0	3
	6	>99		68	2	29	0	1
	10	>99		62	2	35	0	1

[a] Reaction: $[LA]=0.43$ mol L^{-1}; Ru/LA = 1:1000 mol/mol. [b] Converted $mol_{GVL}\,g_{Ru}^{-1}\,h^{-1}$.

action conditions. Such results are of great interest as PA is an important intermediate in the production of biofuels.[4]

The stability of Ru/OMC-P was also investigated at 200 °C and 40 bar H_2 (Figure 6). Under these high-temperature conditions, the catalyst exhibited a lower stability than at 70 °C. The activity decreased slightly during the first three cycles, and a more evident deactivation was observed after the fourth run. The morphology of the nanoparticles changed after five consecutive tests (Figure 2c). Particle size analysis performed by STEM (Table 2) showed that the Ru particles increased in size from 1.6 to 2.5 nm with the formation of some aggregates (Figure 2c). XPS measurements of Ru OMC-P after the catalytic reaction revealed two Ru species with BEs of 283.4 and 280.4 eV attributed to Ru^{6+} and a species that resembles Ru^0 (Figure 3, inset). After the catalytic reaction, there was a clear decrease in the PO_4 concentration (from 0.4 to 0.2 at%) and an increase in Ru concentration (0.4 to 1.2 at%). These results point to the leaching of some of the less stable PO_4 groups, which enabled Ru to migrate to the catalyst surface. Hence, the deactivation of the Ru-OMC-P might be because of the leaching of phosphorylated groups. The role of LA on the deactivation was investigated by testing the catalyst in pure water at 200 °C and $p_{H_2}=40$ bar for 6 h. In this case the deactivation occurred after the first run, which suggests that the deactivation is more because of the harsh reaction conditions than because of the chelating properties of LA.

Conclusions

We demonstrate new Ru supported on ordered mesoporous carbon (OMC) and acid-functionalized OMC (OMC-P and OMC-S) catalysts for the hydrogenation of levulinic acid (LA) under aqueous conditions. The catalytic performance of the Ru nanoparticles was affected greatly by the surface chemistry of the carbon supports. If mild reaction conditions were used (70 °C and 7 bar H_2), the phosphorylated OMCs accelerated the reaction rate, and a high selectivity to γ-valerolactone (GVL; >93%) was observed. Ru/OMC-P has excellent stability and maintains the same activity and selectivity to GVL after five consecutive runs. However, weakly bound surface −S groups leached off the surfaces of OMC-S and bound to the most active Ru nanoparticles, which thus deactivated the Ru catalyst.

Under more severe conditions (200 °C, 40 bar H_2), Ru/OMC-P promoted the further conversion of GVL to pentanoic acid (PA). This conversion did not occur with Ru/OMC. Under these harsh conditions, however, the Ru/OMC-P catalyst starts to deactivate after three consecutive cycles as a result of a combined leaching of weakly bound phosphonic acid groups and a Ru redox reaction with LA. Although the leaching of phosphoric groups may favor the migration of Ru to the more accessible surfaces of the OMC supports, the LA redox reaction promoted the further reduction and aggregation of Ru on the carbon surfaces. These results, however, show a major improvement in the catalyst stability for the conversion of LA in aqueous media compared to those on other acidic oxide supports. The ability to further increase the conversion of GVL to PA is very stimulating and of great interest for the large-scale production of biofuels from PA.

Experimental Section

Materials

$RuCl_3$ (99.99% purity) from Aldrich was used. Gaseous hydrogen from SIAD was 99.99% pure.

Support preparation

Resorcinol (17.6 g) and Pluronic F127 (17.6 g) were dissolved in ethanol (72 mL)/water (54 mL)/HCl (17.6 mL, 12.5 м). Formaldehyde (20.8 mL) was added, and phase separation was observed after 6 min. The gel was stirred for another 60 min. The top liquid phase was separated, and the bottom gel polymer was cast on Mylar. The film was allowed to dry overnight at RT and then at 80 °C for 24 h. The obtained polymer composite was carbonized in flowing Ar (500 mL min^{-1}) at 850 °C for 120 min at a heating rate of 5 °C min^{-1}. This sample was labeled as OMC.

OMC (≈2.5 g) was dispersed in concentrated H_2SO_4 (25 mL) to introduce sulfate groups or in H_3PO_4 (25 mL) to introduce phosphate surface groups. These systems were stirred at 80 °C for 12 h under flowing N_2. The solids were collected by filtration and washed with water until the filtrate was neutral. The samples were dried at 80 °C overnight and labeled as OMC-P and OMC-S after treatment in H_3PO_4 and H_2SO_4, respectively. A batch of the OMC-S material (3.0 g) was stirred in concentrated H_3PO_4 (25 mL) for 6 h at 80 °C under flowing N_2. The solid was recovered by filtration and washed to neutral as with the other samples. This material was labeled OMC-S/P.

Catalyst preparation by incipient wetness impregnation

Solid $RuCl_3$ was dissolved in water ($[Ru]=10$ mg mL^{-1}). Sufficient metal-containing solution was added to each of the OMC supports (OMC, OMC-P, OMC-S, and OMC-P/S) to completely fill their pores, based on the total pore volume from N_2 sorption analysis (Table 1). The amount of support was calculated so that a final Ru loading of 1 wt% was obtained. The catalysts were washed several times with water to remove inorganic residues (Cl^-, Na^+, etc.). The catalyst was then collected by filtration, dried at 80 °C for 2 h, and reduced in H_2 at 200 °C for 2 h. The catalysts were labeled as Ru/OMC, Ru/OMC-P, Ru/OMC-S, and Ru/OMC-P/S.

Catalytic tests

LA hydrogenation was performed in the range of 70–200 °C by using a stainless-steel reactor (30 mL capacity), equipped with a heater, mechanical stirrer, gas supply system, and thermometer. The LA solution (30 mL, 0.43 M) was added to the reactor, and the desired amount of catalyst (LA/metal ratio = 1000 mol/mol) was suspended in the solution. The H_2 pressure was 7 bar.

Before the reaction, the catalyst was pre-reduced in a batch autoclave for 1 h at 150 °C with 3 bars of H_2. The autoclave was then cooled, the H_2 flow was stopped, and the substrate (13.05 mmol LA) and solvent (30 mL H_2O) were loaded. The autoclave was purged three times with N_2 before charging with 7 or 40 bars of H_2. The mixture was heated to the reaction temperature (70 or 200 °C) and stirred mechanically (1250 rpm) for 6 h. At the end of the reaction, the autoclave was cooled, the H_2 flow was stopped, and the autoclave was purged with flowing N_2. The reaction mixture, after separation from the catalysts by filtration, was analyzed by HPLC. Samples were removed periodically (0.5 mL) under stirring and analyzed by HPLC by using an Alltech OA-10308 column (300 mm × 7.8 mm) with UV and refractive index (RI) detection to analyze the product mixtures. A 0.1 % H_3PO_4 solution was used as the eluent. The identification of the possible products was undertaken by comparison with the original samples.

Recycling test

Each run was performed under the same conditions ([LA] = 0.43 mol L^{-1}; Ru/LA = 1:1000 mol/mol, 200 °C, 40 bar H_2). The catalyst was recycled in the subsequent run after filtration without any further treatment.

Characterization

XPS data were collected by using a PHI 3056 spectrometer with an Al anode source operated at 15 kV and an applied power of 350 W. Adventitious carbon was used to calibrate the binding energy shifts of the sample (C 1s BE = 284.8 eV). High-resolution data were collected at a pass energy of 5.85 eV with 0.05 eV step sizes and a minimum of 100 scans to improve the signal-to-noise ratio. Low-resolution survey scans were collected at pass energy of 93.5 eV with 0.5 eV step sizes and a minimum of 25 scans. For the reduction treatments, the samples were loaded in a vacuum furnace located within an Ar-filled glovebox (O_2 < 0.2 ppm; H_2O < 0.1 ppm). The samples were evacuated, then 4 % H_2/Ar was flown over the catalyst surface with heating to 150 °C for 1 h then cooled under H_2/Ar to RT. Samples were pressed manually between two pieces of In foil; the piece of In foil with the sample on it was then mounted on the sample holder with a piece of carbon tape (Nisshin E.M. Co. LTD) and loaded into a vacuum-transfer device used for the analysis of Li metal.[22] The samples were loaded into the spectrometer under vacuum. Peak assignments were made according to phosphorylated carbons[23] and to oxidized carbon nanotubes[24] reported previously.

STEM data were collected on the Ru catalysts by using a Hitachi H3300 STEM operated at 200 kV in the Z-contrast mode, in which the brightness depended on the thickness and approximately the square of the atomic number. Particle sizes were determined by using ImageJ software to process the STEM images. N_2 sorption isotherms were measured at −196 °C by using a TriStar 3000 volumetric adsorption analyzer manufactured by Micromeritics Instrument Corp. (Norcross, GA). Before adsorption measurements, the carbon powders were degassed in flowing N_2 from 1 to 2 h at 200 °C. The specific surface area of the samples was calculated using the BET method within the relative pressure range of 0.05–0.20.[25]

The intrinsic acidity of the carbons was measured by using a METROHM 718 TITRINO. Typically, 100 mg of sample was dispersed in 50 mL of a 10^{-3} M KCl solution. The mixture was stirred vigorously overnight at RT, and the pH of the solution was measured. To quantify the concentration of acid sites, a titration was performed using a 0.01 M NaOH solution on a suspension of 100 mg of carbon in 100 mL of deionized water. Before measurement, the mixtures were degassed under Ar for at least 1 h, until the pH value was constant. The metal content of the catalyst was checked by ICP analysis of the filtrate by using a JobinYvon JY24 instrument and was confirmed to be 1 wt % in all cases.

Acknowledgements

A portion of this research (XPS, OMC synthesis, BET) was supported by the Materials Sciences and Engineering Division, Office of Basic Energy Sciences, U.S. Department of Energy under contract with UT-Battelle, LLC (P.F.F., G.M.V.).

Keywords: carbon · hydrogenation · mesoporous materials · ruthenium · supported catalysts

[1] a) T. Horváth, H. Mehdi, V. Fábos, L. Boda, L. T. Mika, *Green Chem.* **2008**, *10*, 238 – 242; b) D. M. Alonso, S. G. Wettstein, J. A. Dumesic, *Green Chem.* **2013**, *15*, 584 – 595; c) M. Besson, P. Gallezot, C. Pinel, *Chem. Rev.* **2014**, *114*, 1827 – 1870; d) M. J. Climent, A. Corma, S. Iborra, *Green Chem.* **2014**, *16*, 516 – 547; e) W. R. H. Wright, R. Palkovitz, *ChemSusChem* **2012**, *5*, 1657 – 1667.
[2] a) M. Caillon-Caravanier, B. Claude-Montigny, D. Lemordant, G. Bosser, *J. Power Sources* **2002**, *107*, 125 – 132; b) J. Q. Bond, D. Martin Alonso, D. Wang, R. M. West, J. A. Dumesic, *Science* **2010**, *327*, 1110 – 1114; c) J. Q. Bond, D. Martin Alonso, D. Wang, R. M. West, J. A. Dumesic, *J. Catal.* **2011**, *281*, 290 – 299; d) J. C. Serrano-Ruiz, D. J. Braden, R. M. West, J. Dumesic, *Appl. Catal. B* **2010**, *100*, 184 – 189.
[3] H. Mehdi, V. Fabos, R. Tuba, A. Bodor, L. T. Mika, I. T. Horvath, *Top. Catal.* **2008**, *48*, 49 – 54.
[4] J. P. Lange, J. Z. Vestering, R. J. Haan, *Chem. Commun.* **2007**, 3488 – 3490.
[5] O. A. Abdelrahman, A. Heyden, J. Q. Bond, *ACS Catal.* **2014**, *4*, 1171 – 1181.
[6] a) W. H. Luo, U. Deka, A. M. Beale, E. R. H. van Eck, P. C. A. Bruijnincx, B. M. Weckhuysen, *J. Catal.* **2013**, *301*, 175 – 186; b) L. Deng, Y. Zhao, J. Li, Y. Fu, B. Liao, Q. X. Guo, *ChemSusChem* **2010**, *3*, 1172 – 1175; c) Y. Yao, Z. Wang, S. Zhao, D. Wang, Z. Wu, M. Zhang, *Catal. Today* **2014**, *234*, 245 – 250; d) V. Swarna Jaya, M. Sudhakar, S. Naveen Kumar, A. Venugopal, *RSC Adv.* **2015**, *5*, 9044 – 9049.
[7] A. M. Hengne, C. V. Rode, *Green Chem.* **2012**, *14*, 1064 – 1072.
[8] a) L. E. Manzer, *Appl. Catal. A* **2004**, *272*, 249 – 256; b) W. Luo, P. C. A. Bruijnincx, B. M. Weckhuysen, *J. Catal.* **2014**, *320*, 33 – 41.
[9] A. M. Raspolli Galletti, C. Antonetti, V. De Luise, M. Martinelli, *Green Chem.* **2012**, *14*, 688 – 694.
[10] J. C. Serrano-Ruiz, D. Wang, J. A. Dumesic, *Green Chem.* **2010**, *12*, 574 – 577.
[11] a) J.-P. Lange, R. Price, P. M. Ayoub, J. Louis, L. Petrus, L. Clarke, H. Gosselink, *Angew. Chem. Int. Ed.* **2010**, *49*, 4479 – 4483; *Angew. Chem.* **2010**, *122*, 4581 – 4585; b) C. E. Chan-Thaw, M. Marelli, R. Psaro, N. Ravasio, F. Zaccheria, *RSC Adv.* **2013**, *3*, 1302 – 1306.
[12] P. F. Fulvio, R. T. Mayes, X. Wang, S. M. Mahurin, J. C. Bauer, V. Presser, J. McDonough, Y. Gogotsi, S. Dai, *Adv. Funct. Mater.* **2011**, *21*, 2208 – 2215.
[13] R. T. Mayes, P. F. Fulvio, Z. Ma, S. Dai, *Phys. Chem. Chem. Phys.* **2011**, *13*, 2492 – 2494.

[14] M. Kruk, M. Jaroniec, K. P. Gadkaree, *J. Colloid Interface Sci.* **1997**, *192*, 250–256.
[15] M. Jaroniec, L. A. Solovyov, *Langmuir* **2006**, *22*, 6757–6760.
[16] J. Choma, J. Gorka, M. Jaroniec, *Microporous Mesoporous Mater.* **2008**, *112*, 573–579.
[17] W. Wang, S. Guo, I. Lee, K. Ahmed, J. Zhong, Z. Favors, F. Zaera, M. Ozkan, C. S. Ozkan, *Sci. Rep.* **2014**, *4*, 4452.
[18] M. A. Ernst, W. G. Sloof, *Surf. Interface Anal.* **2008**, *40*, 334–337.
[19] C. Moreno-Marrodan, P. Barbaro, *Green Chem.* **2014**, *16*, 3434–3438.
[20] Z. Wu, S. Ge, C. Ren, M. Zhang, A. Yip, C. Xu, *Green Chem.* **2012**, *14*, 3336–3343.
[21] P. Tian, J. Blanchard, K. Fajerwerg, M. Breysse, M. Vrinat, Z. Liu, *Microporous Mesoporous Mater.* **2003**, *60*, 197–206.
[22] L. Baggetto, K. J. Carroll, H.-Y. Hah, C. E. Johnson, D. R. Mullins, R. R. Unocic, J. A. Johnson, Y. S. Meng, G. M. Veith, *J. Phys. Chem. C* **2014**, *118*, 7856–7864.
[23] J. Bedia, J. M. Rosas, J. Marquez, J. Rodriguez-Mirasol, T. Cordero, *Carbon* **2009**, *47*, 286–294.
[24] S. Kundu, Y. Wang, W. Xia, M. Muhler, *J. Phys. Chem. C* **2008**, *112*, 16869–16878.
[25] M. Kruk, M. Jaroniec, *Chem. Mater.* **2001**, *13*, 3169–3183.

Received: March 4, 2015
Revised: April 16, 2015